

Efficient vaccination strategies to reduce the epidemic mortality in population with heterogeneous fatality rate

Bukyoung Jhun^{1,*} and Hoyun Choi¹

¹*CCSS, CTP and Department of Physics and Astronomy, Seoul National University, Seoul 08826, Korea*

An insufficient supply of effective SARS-CoV-2 vaccine in most countries demands an effective vaccination strategy to minimize the damage caused by the disease. Currently, many countries vaccinate their population in descending order of age to minimize the deaths caused by the disease; however, the effectiveness of this strategy needs to be quantitatively assessed. We employed the susceptible-infected-recovered-dead (SIRD) model to investigate various vaccination strategies. In complex network, the case fatality rate (CFR)-based method was shown to be more effective than the load-based strategy when there is a low supply of vaccine; however, when there is a sufficient quantity of vaccine, the load-based strategy is more effective than the CFR-based strategy. We also constructed a metapopulation model with empirical human contact and CFR data for SARS-CoV-2 and investigated vaccination strategies. We found that the age-based strategy, which is currently employed in many countries, is more effective when the basic reproduction number is high and vaccination supply is low, but the rate-based method outperforms the age-based strategy when there is sufficiently high supply of vaccine. Simulated annealing is performed to find the optimal vaccination strategy. We identified a first-order phase transition in the vaccination strategies which is characterized by discontinuous transition in the optimal strategy and the hysteresis. This phase transition implies that mixing the age-based and rate-based strategy is ineffective in reducing the number of deaths. These conclusions are valid even when the heterogeneous degree distribution of human contact is considered.

I. INTRODUCTION

The spreading process in complex networks [1–5] and in the metapopulation [6–10] has been an active field of research for modelling many physical and social phenomena [11–13]. These have included opinion formation in social groups [13–16], the spread of epidemic diseases [6, 17–21], and innovations [22, 23]. A plethora of data [24–26] on human mobility, collaboration, contagion of epidemic disease, and temporal contacts, all of which were previously unavailable to researchers, now enable effective research into various dynamic processes in social systems. Extensive research has been devoted to the spreading processes, providing quantitative analyses for policy-making and especially, in the public health domain. Moreover, the spreading process has provided a deeper understanding of phase transitions and critical behaviors, such as the effect of structural heterogeneity on epidemic thresholds [6, 19, 27] and the hybrid phase transition induced by cascades [28–31].

One of the most important topics in mathematical epidemiology is vaccination strategy, which has been studied with various epidemic models in complex networks and the metapopulation model. If a node in a network is vaccinated, that node will not turn into the infected state even if it is in contact with an infected node. Moreover, when a sufficient fraction of nodes in a network are vaccinated, the infection is unable to spread throughout the network, and the epidemic state is eliminated by the vaccination. This effect is called *herd immunity*. Vaccination strategies frequently aim to achieve herd immunity with the smallest number of vaccine shots.

The SARS-CoV-2 pandemic is ongoing worldwide, and has caused more than four million deaths. Due to the development of effective vaccines for the disease, the elimination of

the disease can be anticipated. However, in most countries, and especially in the developing countries, the number of vaccine shots available is less than the total number of the population [32]. Therefore, it is important to formulate a vaccination strategy that minimizes the damage caused by the disease, such as the number of deaths, with the limited supply of vaccine available. Currently, many countries are vaccinating their populations in descending order of age, since the case fatality rate (CFR) for the SARS-CoV-2 increases with age [33–39]. However, the effectiveness of this strategy needs to be quantitatively assessed.

Here, we introduce the susceptible-infected-recovered-dead (SIRD) model, which is a minimal model to study the death toll caused by an epidemic disease. We evaluate the effectiveness of load-based and CFR-based vaccination strategies in complex networks. We find that if only a small quantity of vaccine is available, the CFR-based strategy will be more effective; however, if sufficient vaccination shots are available, the load-based strategy outperforms the CFR-based strategy. We also employ a metapopulation model with empirical data obtained from previous research (see Sec. IV A for details). We find that an age-based strategy is more effective than the rate-based strategy for a high basic reproduction number and low vaccination supply, but the rate-based strategy outperforms the age-based strategy when sufficiently large amount of vaccine is supplied. Simulated annealing is implemented to find the globally optimal vaccination strategy. We find that there is a first-order phase transition in the vaccination strategy characterized by an abrupt transition in the average age of the vaccinated population and hysteresis. The simulation is performed in a metapopulation with a heterogeneous degree distribution to find that the conclusions from a metapopulation with a homogeneous degree distribution are also valid when a heterogeneity of the degree distribution is considered. Simulated annealing is not implemented for the heterogeneous degree distribution because of the excessively high compu-

* jhunbk@snu.ac.kr

tational cost required.

This paper is organized as follows: First, we introduce the SIRD model in Sec. II. Next, in Sec. III, vaccination strategies that minimize the number of deaths caused by epidemics in complex networks is investigated. In Sec. IV A, we explain the empirical data used to construct the metapopulation model for SARS-CoV-2 epidemics. In Sec. IV B, we investigate the efficiency of vaccination strategies in the metapopulation model constructed from the empirical data, and in Sec. IV C, we study the phase transition of the vaccination strategy. In Sec. IV D, we show that the conclusions from the previous sections are valid even when the heterogeneous degree distribution of human contacts is considered. A summary and final remarks are presented in Sec. V.

II. SUSCEPTIBLE-INFECTED-RECOVERED-DEAD (SIRD) MODEL

The susceptible-infected-recovered (SIR) model is a minimal model of epidemic spreading and the most extensively studied model both in complex networks [17, 18, 27, 40] and in the metapopulation model [6–10], together with its variants [28, 41–46]. In the SIR model, each individual, or node, is in either the susceptible (S), infected (I), or recovered (R) state. A susceptible node can turn into an infected node if it comes into contact with an infected node. The rate of transition is proportional to the number of infected nodes in contact with the node. Infected nodes eventually turn into the recovered state at a constant rate. A recovered node obtains immunity and does not turn into the infected state again. In the real world, actual infectious diseases exhibit more complex stages; however, they can be reduced roughly to the SIR model. Hence, conclusions from a study employing the SIR model should be applicable to actual infectious diseases.

Vaccination strategy is one of the most extensively studied subjects in mathematical epidemiology [47–61]. The objective of vaccination strategies in the SIR model is to minimize the total number of individuals affected by the disease, which can be measured by the number of recovered nodes when the infection vanishes, with limited vaccination resources. However, one of the most important objectives of vaccinations in the real world is to minimize the total number of deaths caused by a disease. Since there is no state or process that represents death in the SIR model, the model cannot be used to study vaccination strategies relating to such a purpose. At this point, we introduce the susceptible-infected-recovered-dead (SIRD) model, which is a minimal model that also includes cases of mortality. By the same spirit of the SIR model, it should be possible to reduce the complex stages exhibited by the actual disease to the SIRD model; hence, the results of this research should be valid for actual infectious diseases.

In the SIRD model, similar to the SIR model, each node is in either a susceptible (S), infected (I), recovered (R), or dead (D) state. If a susceptible node and an infected node are in contact (connected by a link in the network), the susceptible node is turned into the I state at rate η (it turns with probability $\eta\Delta t$ in an infinitesimal time step Δt). If the S node is in contact

with n infected nodes, the rate becomes $n\eta$. Any node that is in the I state turns into the R state at rate μ , or into the D state at rate $\kappa\mu$. The rate equation for the SIRD model is, therefore,

$$S + I \xrightarrow{\eta} I + I, \quad (1)$$

$$I \xrightarrow{\mu} R, \quad (2)$$

$$I \xrightarrow{\kappa\mu} D, \quad (3)$$

where η is the contagion rate, μ is the recovery rate, and κ is a non-negative parameter that controls the case fatality rate (CFR) of the disease. The CFR is defined as the ratio of deaths from a certain disease compared to the total number of people diagnosed with the disease. The R state and D state appears with ratio $\kappa : 1$. Therefore, the CFR for the SIRD model is

$$\text{CFR} = \frac{\kappa}{1 + \kappa}, \quad (4)$$

which is always between zero and one for non-negative κ .

If the contagion rate of an epidemic disease is higher than a threshold, an epidemic outbreak that starts from a single node can spread over an entire network. One way to parametrize epidemics is through the basic reproduction number [62–64], which is usually denoted as R_0 . The basic reproduction number is the anticipated number of contagions caused by a single infected individual until the individual becomes unable to spread the infection anymore, due to either recovery or death. If $R_0 > 1$ at $t = 0$, on average, a single infected node will spread the infection to more than one node; thus, the infection will spread. Therefore, the threshold of an epidemic can be expressed as $R_0 = 1$. Initially, only an infinitesimal proportion of the nodes are infected; therefore, the basic reproduction number can be expressed as

$$R_0 = \frac{\eta}{\mu} \bar{\Lambda}, \quad (5)$$

where $\bar{\Lambda}$ is the largest eigenvalue of the modified adjacency matrix $a_{ij}/(1 + \kappa_j)$ for network and $M_{ij}/(1 + \kappa_j)$ for metapopulation. a_{ij} is the adjacency matrix of the network and M_{ij} is the contact matrix (see Sec. IV B for details) of the metapopulation model.

III. VACCINATION STRATEGIES IN NETWORKS

A. Method

The Gillespie algorithm [65, 66] performs efficient and exact Monte Carlo simulations for stochastic processes in continuous time. The probability distribution of the Gillespie algorithm is identical to the theoretical distribution of the stochastic process: the method is thus *stochastically exact*. We employ the Gillespie algorithm to simulate the SIRD model in networks.

Initially, all nodes are in the susceptible state except for one node, which is in the infected state. We simulate the dynamics with the Gillespie algorithm until there are no infected nodes.

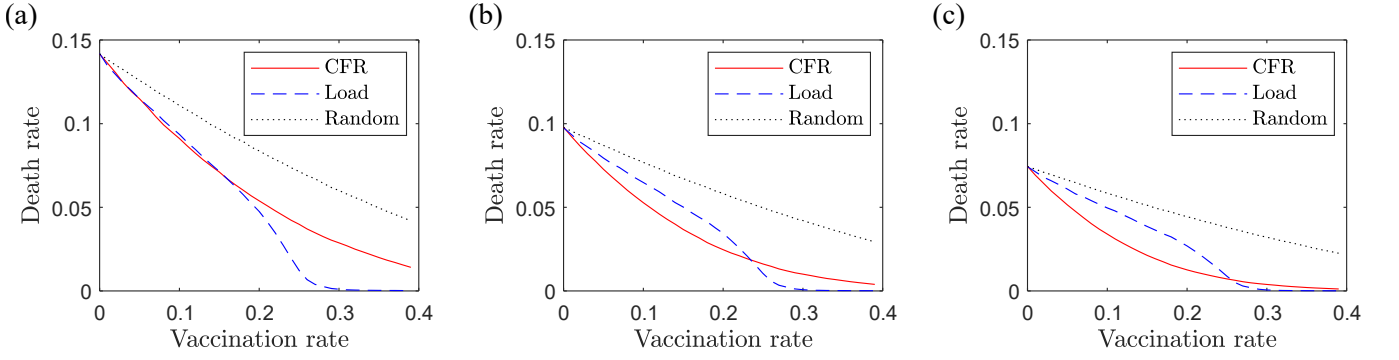


FIG. 1. The death rate in the static model under various vaccination strategies. The κ of each node is independently drawn from the distribution Eq. (6) with (a) $\theta = 3$, (b) $\theta = 5$, and (c) $\theta = 7$. A high value of θ results in a highly heterogeneous CFR distribution. As the CFR of the nodes become more heterogeneous, the CFR-based strategy becomes more efficient compared to the load-based method. However, when sufficiently large vaccine supply is provided, the load-based strategy outperforms the CFR-based method. The random vaccination strategy is plotted as a benchmark.

Because all the reactions in Eqs. (1)–(3) involve an infected node; the state of any one node does not change any more. We iterate the process for 2×10^5 with a single infection seed and calculate the average number of nodes in the D state at the end. To generate networks that have the properties of real-world networks, we use the static model [67–69], which has been used to study many dynamic processes in complex networks owing to its simplicity and analytical tractability [69–72]. In the static model, each of the N nodes in the network is first assigned a fitness q_i . Second, a link is added between two nodes i and j with the probability $q_i q_j$. Then, we repeat the second step for NL times. If we take $q_i = i^\mu / \zeta_N(\mu)$, where $\zeta_N(\mu) = \sum_{j=1}^N j^{-\mu}$, the resulting network has an average degree $\langle k \rangle = 2L$ and a power-law degree distribution of $P(k) \sim k^{-\gamma}$ with exponent $\gamma = 1 + 1/\mu$.

The CFR of each node is drawn independently from the distribution

$$P(\kappa) = \frac{1}{\theta} \kappa^{-\frac{\theta-1}{\theta}} I_{(0,1)}(\kappa), \quad (6)$$

where $I_{(0,1)}(\kappa) = 1$ for $0 < \kappa < 1$ and otherwise $I_{(0,1)}(\kappa) = 0$. The parameter θ controls the heterogeneity of the distribution, where a large θ reflects a highly heterogeneous distribution. A random number can be generated from the distribution as $\kappa = u^\theta$, where $u \sim \mathcal{U}(0, 1)$ is a uniform random number between zero and one.

B. Results

We implemented the SIRD model for three vaccination strategies aimed at minimizing deaths caused by epidemics: the CFR-based method, the load-based method, and random vaccination. In the CFR-based method, we vaccinate the nodes with the highest CFR, or equivalently, the highest κ . The vaccinated nodes remain in the S state, even if they contact with an infected node. The load-based method vaccinates the nodes with the highest load [67, 71]. Load is a measure of the centrality of a node in a network, based on the num-

ber of shortest paths between all pairs of nodes in the network that pass through the node. The load-based method is independent of the CFRs of each node and has been found to be effective for containing SIR epidemics in complex networks [50, 52, 60]. We also simulated random vaccination strategy, which vaccinates random nodes, as a baseline.

We performed numerical simulations in the static model with an average degree $\langle k \rangle = 8$ and the degree exponent $\gamma = 3$. We used various values of θ to see the effects of the heterogeneity of the CFR on the results. We plotted the mortality rate, or the death rate, which is the expected fraction of nodes in the D state when the epidemic stops in the network, in Fig. 1 for $\theta = 3$, $\theta = 5$, and $\theta = 7$. The parameters were fixed to $\eta = 2$ and $\mu = 1$. Note that a highly heterogeneous fatality rate (a large θ) gave advantage to the CFR-based method compared to the load-based method. However, for sufficiently high vaccination supply, which is the fraction of nodes that are vaccinated, the load-based method outperformed the CFR-based strategy.

IV. VACCINATION STRATEGIES IN THE METAPOPOPULATION

A. Empirical data

The contact matrix $M_{\alpha\beta}$ is defined as the average contacts that an individual in group α has with the individuals in group β . Contact data between each age group in 35 countries has been studied by means of survey [73]. While the data is available for many countries, here, we use the data from the United States. The contact matrix of the United States population for each age group is illustrated in Fig. 2(a). The population is divided into 9 groups: aged 0–9, 10–19, ..., 70–79, and above 80. Contact within the similar age group is disproportionately intense, and contacts between teenagers exhibit the highest strength.

The CFR of SARS-CoV-2 is an active topic of research [33–37, 39]. Here, we use an up-to-date estimation of the CFR in

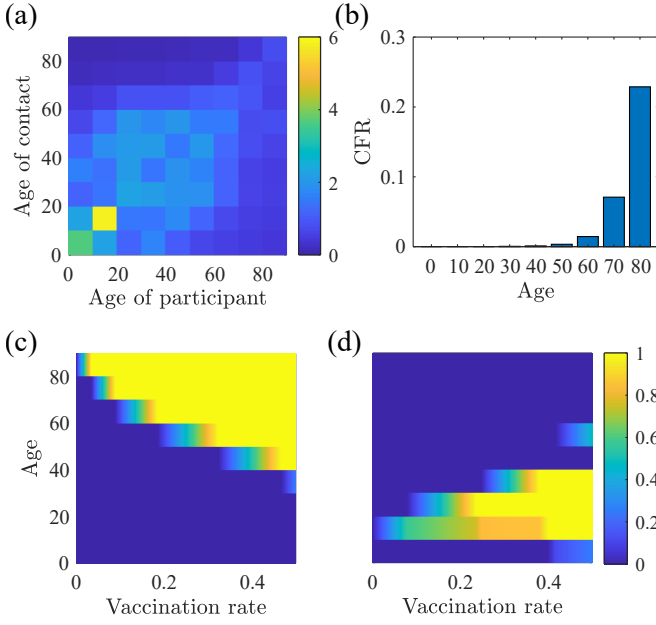


FIG. 2. (a) The age contact matrix of the population of the United States. The population is divided into 9 groups: aged 0–9, 10–19, ..., 70–79, and above 80. The interaction strength between groups of similar age is disproportionately higher, and groups of ages 10–29 show the highest number of contacts. (b) Case fatality rate (CFR) and κ of the SARS-CoV-2 in each age group of the South Korean population. CFR is highly heterogeneous and monotonically increases with age. The fraction of individuals vaccinated by the (c) age-based and (d) rate-based strategy for various vaccination rates. The age groups 10–19 and 20–29 are primarily vaccinated by the rate-based strategy.

South Korea [38]. Intensive contact tracing and testing, often referred to as the K-quarantine model [74–80], together with the small number of cases, results in an accurate estimation of the CFR. The estimated CFR for each age group in South Korea is illustrated in Fig. 2(b). This composition of population results in high epidemic mortality rate: if the population consist solely of young people, almost no people will die because of their extremely low CFR, and if there are only senior population, the epidemics cannot spread through the population because of their low contact rate.

B. Homogeneous degree distribution

In the metapopulation model, the population is divided into a number of groups. We use the interaction strength between each group, including interaction within the same group, to study the dynamic processes. The epidemic equation for the

SIRD model in the metapopulation model is

$$\frac{\partial}{\partial t} P_{\alpha}^I(t) = \eta P_{\alpha}^S(t) \sum_{\beta} M_{\alpha\beta} P_{\beta}^I(t) - \mu(1 + \kappa_{\alpha}) P_{\alpha}^I(t), \quad (7)$$

$$\frac{\partial}{\partial t} P_{\alpha}^R(t) = \mu P_{\alpha}^I(t), \quad (8)$$

$$\frac{\partial}{\partial t} P_{\alpha}^D(t) = \mu \kappa_{\alpha} P_{\alpha}^I(t), \quad (9)$$

where P_{α}^S , P_{α}^I , P_{α}^R , and P_{α}^D are the probability that an individual in group α is in the S, I, R, or D state, respectively. The set of differential equations (Eqs. (7)–(9)) can be numerically solved by the Runge-Kutta method [81, 82].

Initially, an infinitesimal fraction, $n_0 = 10^{-8}$ of each group α of the population, is in the I state, and all the rest of the population $1 - n_0$ is in the S state. The differential equations are then solved by fourth order Runge-Kutta method until the total proportion of infected individuals $\sum_{\alpha} \sum_{\beta} M_{\alpha\beta} P_{\beta}^I$ becomes less than a certain threshold 10^{-12} . We then calculate the total proportion of the dead population $\sum_{\alpha} \sum_{\beta} M_{\alpha\beta} P_{\beta}^D$. Unlike the SIRD model in the network, this model is deterministic. Therefore, the equations need to be solved just once for a set of parameters.

We implement four vaccination strategies: age-based, rate-based, simulated annealing, and random vaccination strategy. Since the CFR of the SARS-CoV-2 monotonically increases with age, in the age-based method, we vaccinate the population in descending order of age (Fig. 2(c)). In the rate-based method, infinitesimal amount of vaccine is given to the age group with the highest contact rate $\sum_{\beta} M_{\alpha\beta}$. Then, the modified contact rates are defined as $\sum_{\beta} M_{\alpha\beta} (1 - v_{\beta})$, where v_{β} is the fraction of vaccinated individuals in the group β . Another infinitesimal vaccine is repeatedly distributed based on the new contact rates. The age group vaccinated by the rate-based strategy is illustrated in Fig. 2(d). The population aged 10–29 is primarily vaccinated by this strategy because of their high contact rate.

The simulated annealing is a probabilistic optimization algorithm inspired by spin glass [83]. We implemented a modified version of the simulated annealing technique to find the globally optimal vaccination strategy. First, we started with random vaccination strategy with a certain level of vaccine supply, which is the fraction of the vaccinated individual in the entire population. We set this strategy as a provisional solution. Then we calculated the death rate of a trial strategy, which is perturbed from the provisional solution by a small amount, while keeping the vaccine supply of the total population constant. If the death rate of the trial strategy is smaller than that of the provisional solution, we replace the provisional solution with the trial strategy. Otherwise, we replace the provisional solution with the trial strategy with probability $\exp(-1/T)$, where T is the temperature of the algorithm. At the beginning, the temperature is set at $T = 2$. We iterate this process for $n_{\text{iter}} = 10^6$ times, while the temperature is dropped by a factor $f_{\text{iter}} = 1 - 10^{-5}$ at each step. The resulting provisional solution is the optimal vaccination strategy, given that n_{iter} is sufficiently large and f_{iter} is sufficiently close to one.

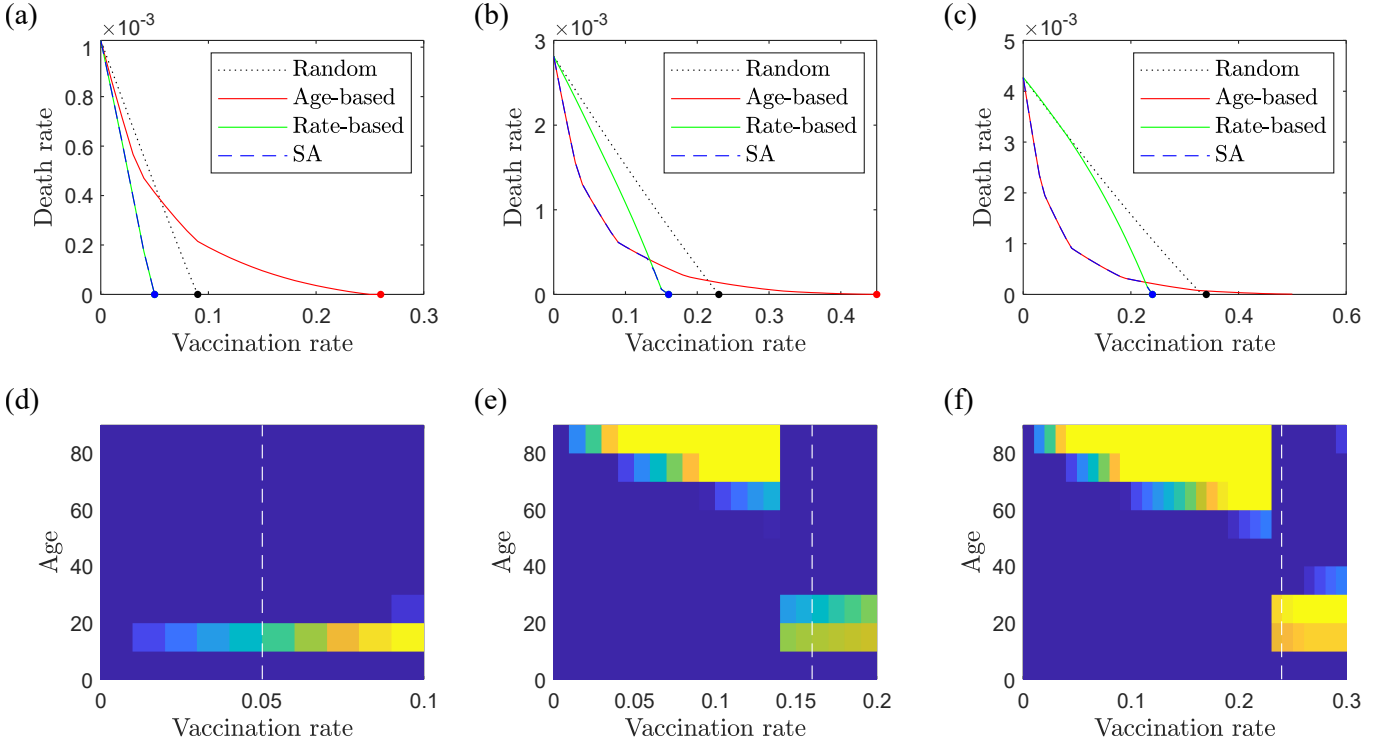


FIG. 3. (a–c) The death rate as a result of various vaccination strategies. The simulation was performed for various basic reproduction numbers: (a, d) $R_0 = 1.1$ ($\eta = 0.094264$), (b, e) $R_0 = 1.3$ ($\eta = 0.111403$), and (c, f) $R_0 = 1.5$ ($\eta = 0.128542$). When the fraction of the population affected by the epidemic, which is the fraction of the R and D state at the end of the dynamic, is less than 10^{-4} , we assume that herd immunity is achieved, and the epidemic is eliminated by vaccination. The point at which herd immunity is achieved is depicted as a dot. (d–f) The fraction of the population in each group vaccinated by the optimal strategy is found by simulated annealing. The dashed white line is the threshold for herd immunity. In (d), the method involves vaccinating the teenagers, and shows no complex behavior. However, there is an abrupt transition of strategy in (e) and (f). For a low vaccine supply, the method involves vaccinating the senior population, but for sufficiently large vaccine supply, the young population is primarily targeted for vaccination. This abrupt transition of the strategy indicates a first-order phase transition.

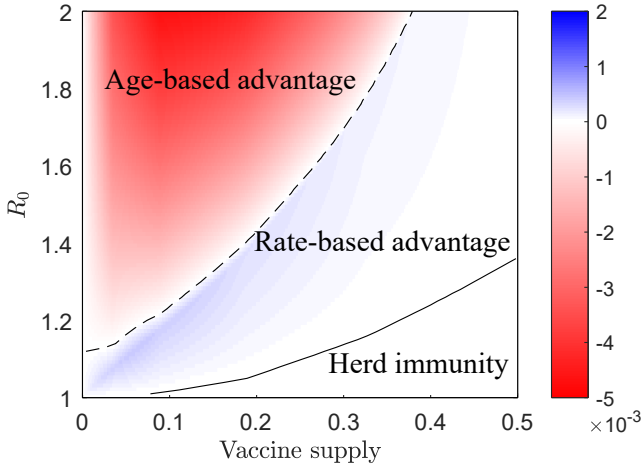


FIG. 4. The difference between the death rate resulting from age-based and rate-based strategies. The dashed line represents the boundary between the regions where the age- and rate-based strategies are advantageous in reducing the death rate. The age-based strategy reduces more deaths than the rate-based strategy when the basic reproduction number R_0 is high and the level of vaccine supply is low. However, as the vaccine supply becomes higher, the rate-based strategy outperforms the age-based strategy.

The random vaccination strategy homogeneously vaccinates the population regardless of their age.

We performed numerical simulations using the contact matrix and the CFR data explained in the previous section. The death rates resulting from the strategies are illustrated in Fig. 3(a–c). If the fraction of nodes in the R or D state at the end of the epidemic process is less than 10^{-4} , we assume that herd immunity is achieved and that the epidemic is eliminated by the vaccination. The age-based strategy is advantageous over the rate-based strategy for large R_0 and a small vaccine supply; however, for sufficiently large vaccine supply, the rate-based strategy outperforms the age-based strategy. For a large vaccine supply, the age-based strategy is even less efficient than the random vaccination strategy. This is because the senior population targeted by the age-based strategy has low contact rate, therefore, vaccinating them is ineffective in obtaining herd immunity. The optimal strategy found by the simulated annealing exhibits mortality rate close to one for the age-based or rate-based strategies. This suggests that the globally optimal strategy is close to one of these two strategies. The population targeted by the optimal strategy is illustrated in Fig. 3(d–f). The dashed white line in the figure marks the point at which herd immunity is achieved by the optimal strategy. There is a sharp transition of the strategy in Fig. 3(e, f),

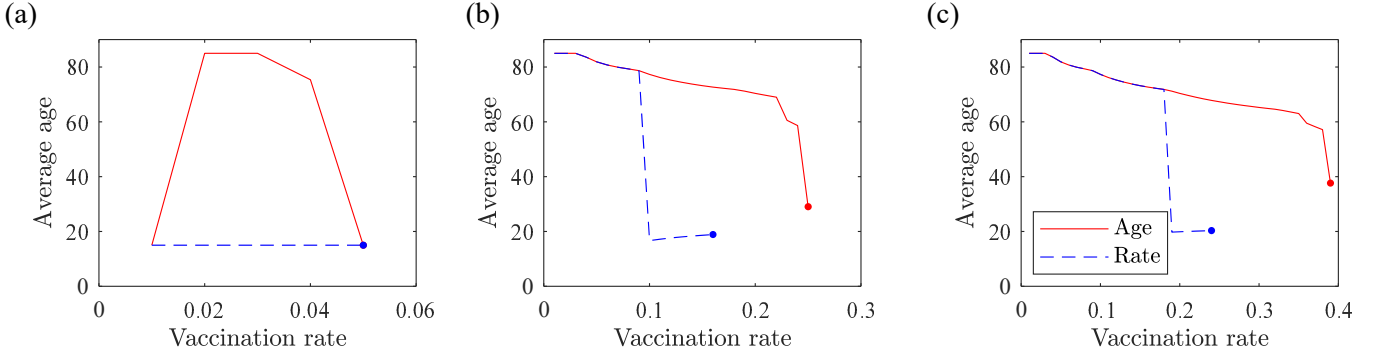


FIG. 5. The average age of the vaccinated individuals of the vaccination strategies found by the zero-temperature simulated annealing with the initial state (strategy) of age- (solid red line) and rate-based methods (dashed blue line). The basic reproduction numbers are (a) $R_0 = 1.1$ ($\eta = 0.094264$), (b) $R_0 = 1.3$ ($\eta = 0.111403$), and (c) $R_0 = 1.5$ ($\eta = 0.128542$). The dot represents the point where herd immunity is achieved and the endemics is eliminated by the vaccination. For small vaccination rate, the results of the zero-temperature simulated annealing started from two methods coincide, however, for sufficiently large vaccine supply, the two strategies show a largely unequal average age of the vaccinated population. The abrupt change of the average age at the transition point and the hysteresis suggests that the phase transition is of first-order.

suggesting the existence of a discontinuous phase transition in the vaccination strategy.

The difference between the death rates of age- and rate-based strategies for various vaccine supply and R_0 is illustrated in Fig. 4. When $R_0 < R_0^* = 1.12$, the rate-based strategy outperforms the age-based strategy for all levels of vaccine supply. When $R_0 > R_0^*$, the age-based strategy is advantageous for low vaccine supply; however, when the vaccine supply is above a critical value, which is depicted as a dashed line in the figure, the rate-based strategy reduces more deaths than the age-based strategy. The solid line shows where the both strategies achieve the herd immunity hence the difference between the strategies becomes irrelevant.

C. Phase transition

In this section, we further investigate the nature of phase transition suggested by Fig. 3(e) and (f). To find locally optimal solutions, we use the zero-temperature simulated annealing, which is analogous to the gradient-descent method. Initially, the provisional solution is set to the age-based or rate-based strategy. Then, we perturb the provisional solution by decreasing the vaccination rate of group α by $\delta v/P(\alpha)$ and increasing the vaccination rate of group β by $\delta v/P(\beta)$, where δ is a small number and $P(\alpha)$ is the portion of the group α in the population. This way, the total vaccination rate of the entire population remains constant. Among perturbed solutions, if any solution results in a smaller death rate, we replace the provisional solution with the perturbed solution that results in the smallest death rate. Otherwise (i.e. if all the perturbed solutions result in larger death rates than the provisional solution), we have achieved a locally optimal solution, and hence we terminate the process.

We searched for a locally optimal solution in the vicinity of the age-based and rate-based strategy for the metapopulation model studied in Sec. IV.3. We illustrate the average age of the vaccinated population for the locally optimal solution

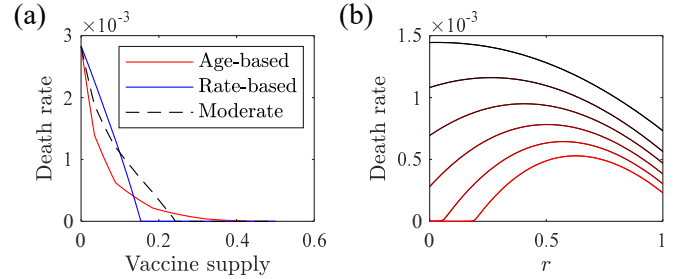


FIG. 6. (a) The death rate as a result of age-based, rate-based, and the moderate strategies. The moderate strategy is a mixed strategy of the age- and rate-based strategies with $r = 0.5$. The moderate strategy is never an optimal strategy and less efficient than both of the strategies in some interval. (b) The death rate of the moderate strategy of age- and rate-based strategy for $R_0 = 1.3$ and vaccine supply, from top to bottom, 8%, 10%, 12%, 14%, 16%, and 18%. There is a barrier of death rate between the age- and rate-based strategy, which is the cause of the hysteresis of the phase transition. The death rate of the rate-based strategy drops faster than the rate-based strategy as the level of vaccine supply increases, causing the crossover between the two strategies.

obtained with the initial state of the age-based and rate-based strategy in Fig. 5. This value serves as the order parameter of the phase transition. The two results coincide at low levels of vaccine supply, suggesting that there is a single globally optimal strategy in the system. However, for sufficiently large vaccine supply, the two results are distinct, i.e., the system exhibits hysteresis. This suggests that there are two locally optimal strategies in the system. The average age of the solution changes discontinuously at the transition point. The hysteresis and the abrupt change of the average age of vaccinated individuals suggest that the phase transition is of first-order.

The hysteresis of this phase transition implies that the moderate strategy of the age- and rate-based strategy is less effective than both of the strategies. The vaccination rate of the moderate strategy is $v_{\alpha}^{\text{mod}} = r v_{\alpha}^{\text{age}} + (1 - r) v_{\alpha}^{\text{rate}}$, where v_{α}^{age} and

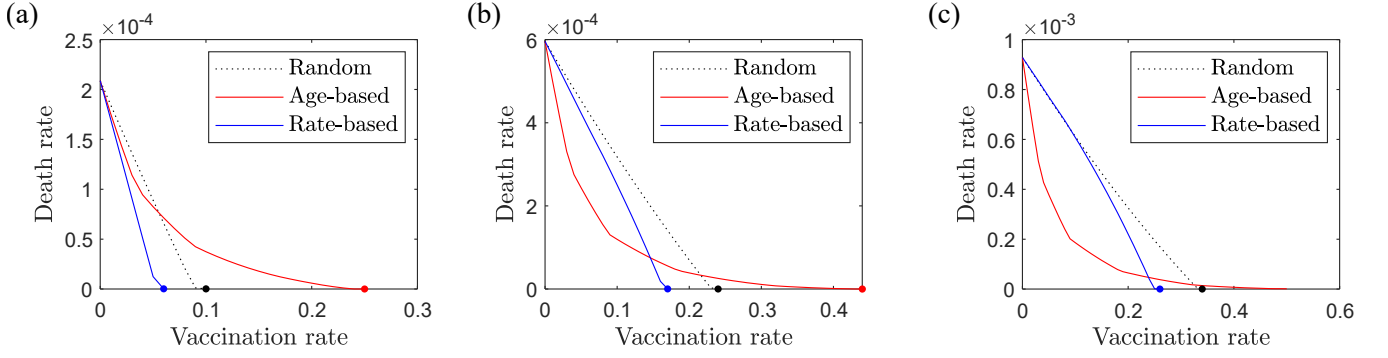


FIG. 7. The death rate as a result of the random (dotted black line), age-based (solid red line), and rate-based vaccination strategy. The basic reproduction numbers of the epidemics are (a) $R_0 = 1.1$ ($\eta = 0.026778$), (b) $R_0 = 1.3$ ($\eta = 0.031705$), and (c) $R_0 = 1.5$ ($\eta = 0.036516$). The rate of recovery is set $\mu = 1$. If the fraction of the nodes affected by the infection, which is the density of nodes that are in R or D state at the end of the epidemics, is below 10^{-4} , we assume that the epidemic is eliminated by the vaccination and herd immunity is achieved. Such a point is depicted as a dot in each plot. For large R_0 , the age-based strategy outperforms the rate-based strategy for a low level of vaccine supply; however, for a sufficiently high level of vaccine supply, the rate-based method outperforms the age-based strategy and achieves the herd immunity at lower vaccination rate.

v_{α}^{rate} are vaccination rates of the age group α decided by the age- and rate-based strategy, respectively. The performance of the moderate strategy for various level of vaccine supply is depicted in Fig. 6(a). The dashed line is moderate strategy with ratio $r = 0.5$ of the age- and rate-strategy. The moderate strategy is never more effective than both the age- and rate-based strategy, and in some region, it is less effective than both of the strategies. Illustrated in Fig. 6(b) is the performance of the moderate strategy versus the ratio r . The basic reproduction number $R_0 = 1.3$ and the total vaccine supply ranges from 8% to 18%. There is a barrier of death rate between the strategy, which is the origin of the hysteresis. The death rate of the rate-based strategy ($r = 0$) decreases faster than the age-based strategy ($r = 1$) and achieves zero death rate at a lower level of vaccine supply.

D. Heterogeneous degree distribution

It was reported that the degree distribution of contact between individuals is not homogeneous, but follows a negative binomial distribution NB(r, p) with $r \simeq 0.36$ [84]. The parameter p_{β} of the age group β can be determined by the average degree $\langle k \rangle_{\beta} = \sum_{\alpha} M_{\alpha\beta}$: $p_{\beta} = 1 - \langle k \rangle_{\beta} / (r + \langle k \rangle_{\beta})$. Then the differential equations (Eqs. (7)–(9)) become

$$\frac{\partial}{\partial t} P_{\alpha k}^I(t) = \eta P_{\alpha k}^S(t) \sum_{\beta} \sum_{k'} M_{\alpha\beta} \frac{kk'}{\langle k \rangle_{\alpha} \langle k \rangle_{\beta}} P_{\beta k'}^{(\beta)} P_{\alpha k}^I(t) - \mu (1 + \kappa_{\alpha}) P_{\alpha k}^I(t), \quad (10)$$

$$\frac{\partial}{\partial t} P_{\alpha k}^R(t) = \mu P_{\alpha k}^I(t), \quad (11)$$

$$\frac{\partial}{\partial t} P_{\alpha k}^D(t) = \mu \kappa_{\alpha} P_{\alpha k}^I(t), \quad (12)$$

where $P_d^{(\alpha)}(k)$ is the degree distribution of the age group α . $P_{\alpha k}^S$, $P_{\alpha k}^I$, $P_{\alpha k}^R$, and $P_{\alpha k}^D$ are the probability that an individual

with degree k in group α is in the S, I, R, or D state, respectively. We track $P_{\alpha k}^S$, $P_{\alpha k}^I$, $P_{\alpha k}^R$, and $P_{\alpha k}^D$ for each α and $k = 0, 1, \dots, 99$. Initially, an infinitesimal portion $n_0 = 10^{-8}$ of each group (α, k) of the population is in the I state and all the rest of the population $1 - n_0$ is in the S state. Then, the differential equations are solved by the fourth order Runge-Kutta method until the total portion of the infected individuals $\sum_{\alpha} \sum_{\beta} \sum_k M_{\alpha\beta} P_d^{(\beta)}(k) P_{\beta k}^I$ becomes less than a certain threshold 10^{-12} .

The death rate resulting from the random, age-based, and rate-based strategies in the metapopulation model with heterogeneous degree distribution is illustrated in Fig. 7. The conclusions from the previous section hold even when the heterogeneity of the degree distribution is considered. A large R_0 gives the advantage to the age-based strategy relative to the rate-based strategy; however, the rate-based method outperforms the age-based method for sufficiently large vaccine supply. The rate-based strategy achieves herd immunity at a lower vaccination rate. The simulated annealing was not performed due to the excessively large computational cost required for the heterogeneous degree distribution.

V. CONCLUSION

In summary, we introduced the SIRD model to investigate the effectiveness of vaccination strategies to minimize the death rate in complex networks and metapopulation. In a complex network, we tested two vaccination strategies, the load-based strategy and CFR-based strategy, together with random vaccination. The load-based strategy vaccinates the nodes with descending order of their load, and the CFR-based strategy vaccinates nodes in descending order of their CFR. A highly heterogeneous CFR distribution is more advantageous to the CFR-based strategy compared to the load-based method, and the CFR-based strategy is more effective than the load-based strategy when the vaccination supply is low.

However, when sufficiently large amount vaccine supply is available, the load-based strategy outperforms the CFR-based strategy.

Vaccination strategies were also evaluated in the metapopulation model constructed from a survey of human contacts and an up-to-date estimation of the CFR for SARS-CoV-2. We investigated the age-based, rate-based, and simulated annealing strategies, together with random vaccination as a benchmark. The age-based strategy vaccinates the population in descending order of age, and the rate-based strategy vaccinates first the age groups with the highest contact rate. As a result, the rate-based strategy primarily vaccinates the population of ages 10–29 because of their high contact rate. Simulated annealing was employed to find globally optimal vaccination strategies. The age-based strategy is more effective than the rate-based strategy for a high basic reproduction number with a low level of vaccine supply; however, the rate-based strategy outperforms the age-based strategy when high level of vaccine supply is available and eventually achieves herd immunity at a lower vaccine supply. We found that there is a first-order phase transition in the optimal vaccination strategy which is characterized by a discontinuous transition of globally optimal strategy and hysteresis. The hysteresis of this phase transition implies that mixing these two strategies is ineffective in reducing the death rate of the epidemic disease. Therefore, if a country has implemented an age- or rate-based strat-

egy, changing the strategy to the other would not be effective. These conclusions are also valid when the heterogeneous degree of distribution of human contact is considered.

In conclusion, the effectiveness of vaccination strategies is closely related to the amount of vaccine available. Hence, the quantity of vaccine supply should be estimated before the design of the vaccination strategies. Precise estimation of the contact matrix, basic reproduction number, and the CFR of the population is also important. In the survey data used in this paper, all types of contacts are treated equally. However, the contagion rate of a disease between individuals who live in the same house, work in the same place, or shop in the same grocery store should differ from each other. If more accurate contagion tree data of the disease is collected and implemented, the relative strength of such interactions will be taken into account. Although the effectiveness of the strategies at specific vaccination rate can be more accurately predicted if the precision of the dataset is improved, because the nature of the phase transition is invariant under perturbations, the phenomena observed in this paper and the conclusions should still be valid.

ACKNOWLEDGMENTS

This research was supported by the NRF, Grant No. NRF-2014R1A3A2069005.

-
- [1] S. N. Dorogovtsev, A. V. Goltsev, and J. F. F. Mendes, *Rev. Mod. Phys.* **80**, 1275 (2008), arXiv:0705.0010.
 - [2] M. G. Zimmermann, V. M. Eguíluz, and M. San Miguel, *Phys. Rev. E* **69**, 065102(R) (2004), arXiv:0405370 [cond-mat].
 - [3] S. N. Dorogovtsev and J. F. F. Mendes, *Adv. Phys.* **51**, 1079 (2002), arXiv:0106144 [cond-mat].
 - [4] K. Klemm, V. M. Eguíluz, R. Toral, and M. San Miguel, *Phys. Rev. E* **67**, 026120 (2003), arXiv:0210542 [cond-mat].
 - [5] M. Nekovee, Y. Moreno, G. Bianconi, and M. Marsili, *Phys. A Stat. Mech. its Appl.* **374**, 457 (2007), arXiv:0807.1458.
 - [6] D. J. Watts, R. Muhamad, D. C. Medina, and P. S. Dodds, *Proc. Natl. Acad. Sci. U. S. A.* **102**, 11157 (2005).
 - [7] V. Colizza and A. Vespignani, *Phys. Rev. Lett.* **99**, 148701 (2007), arXiv:0802.3636.
 - [8] V. Colizza and A. Vespignani, *J. Theor. Biol.* **251**, 450 (2008), arXiv:0706.3647.
 - [9] A. L. Lloyd and V. A. Jansen, *Math. Biosci.* **188**, 1 (2004).
 - [10] N. Masuda, *New J. Phys.* **12**, 10.1088/1367-2630/12/9/093009 (2010).
 - [11] H. Hoang and B. Antoncic, *J. Bus. Ventur.* **18**, 165 (2003).
 - [12] M. E. Newman, *SIAM Rev.* **45**, 167 (2003), arXiv:0303516 [cond-mat].
 - [13] S. Boccaletti, V. Latora, Y. Moreno, M. Chavez, and D.-U. Hwang, *Phys. Rep.* **424**, 175 (2006).
 - [14] D. Acemoğlu, G. Como, F. Fagnani, and A. Ozdaglar, *Math. Oper. Res.* **38**, 1 (2013).
 - [15] A. Grabowski and R. A. Kosiński, *Phys. A Stat. Mech. its Appl.* **361**, 651 (2006).
 - [16] D. J. Watts and P. S. Dodds, *J. Consum. Res.* **34**, 441 (2007).
 - [17] Y. Moreno, R. Pastor-Satorras, and A. Vespignani, *Eur. Phys. J. B* **26**, 521 (2002), arXiv:0107267 [cond-mat].
 - [18] C. Ji and D. Jiang, *Appl. Math. Model.* **38**, 5067 (2014).
 - [19] R. Pastor-Satorras and A. Vespignani, *Phys. Rev. E - Stat. Physics, Plasmas, Fluids, Relat. Interdiscip. Top.* **63**, 066117 (2001), arXiv:0102028 [cond-mat].
 - [20] A. S. Mata and S. C. Ferreira, *Epl* **103**, 48003 (2013), arXiv:1305.5153.
 - [21] G. F. de Arruda, G. Petri, F. A. Rodrigues, and Y. Moreno, *Phys. Rev. Res.* **2**, 013046 (2020), arXiv:1812.04734.
 - [22] Z. Katona, P. P. Zubecek, and M. Sarvary, *J. Mark. Res.* **48**, 425 (2011).
 - [23] E. M. Rogers, *J. Health Commun.* **9**, 13 (2004).
 - [24] J. Jia and A. R. Benson, in *Proc. Twelfth ACM Int. Conf. Web Search Data Min.* (ACM, New York, NY, USA, 2019) pp. 366–374.
 - [25] J. Leskovec, J. Kleinberg, and C. Faloutsos, *ACM Trans. Knowl. Discov. Data* **1**, 10.1145/1217299.1217301 (2007), arXiv:0603229 [physics].
 - [26] J. H. Fowler, *Polit. Anal.* **14**, 456 (2006).
 - [27] R. Pastor-Satorras and A. Vespignani, *Phys. Rev. Lett.* **86**, 3200 (2001), arXiv:0010317 [cond-mat].
 - [28] W. Choi, D. Lee, and B. Kahng, *Phys. Rev. E* **95**, 022304 (2017), arXiv:1608.02323.
 - [29] D. Lee, W. Choi, J. Kertész, and B. Kahng, *Sci. Rep.* **7**, 1 (2017).
 - [30] D. Lee, S. Choi, M. Stippinger, J. Kertész, and B. Kahng, *Phys. Rev. E* **93**, 042109 (2016), arXiv:1512.08335.
 - [31] B. Jhun, M. Jo, and B. Kahng, *J. Stat. Mech. Theory Exp.* **2019**, 123207 (2019), arXiv:1910.00375.
 - [32] M. Tatar, J. M. Shoorekchali, M. R. Faraji, and F. A. Wilson, *J.*

- Glob. Health **11**, 03086 (2021).
- [33] W. Li, R. Thomas, H. El-Askary, T. Piechota, D. Struppa, and K. A. Abdel Ghaffar, *Earth Syst. Environ.* **4**, 513 (2020).
 - [34] A. T. Levin, W. P. Hanage, N. Owusu-Boaitey, K. B. Cochran, S. P. Walsh, and G. Meyerowitz-Katz, *Eur. J. Epidemiol.* **35**, 1123 (2020).
 - [35] B. Manuel, K. Richard, T.-s. Sarah, H. H. H. W. A. F, and N. R. A, *Swiss Med Wkly* **150**, 2019 (2020).
 - [36] F. Barone-Adesi, L. Ragazzoni, and M. Schmid, *Disaster Med. Public Health Prep.* **14**, E1 (2020).
 - [37] D. H. Kim, Y. J. Choe, and J. Y. Jeong, *J. Korean Med. Sci.* **35**, 1 (2020).
 - [38] E. Shim, *Int. J. Environ. Res. Public Health* **18**, 10.3390/ijerph18105053 (2021).
 - [39] T. Bhatt, V. Kumar, S. Pande, R. Malik, A. Khamparia, and D. Gupta, *Stud. Comput. Intell.* **924**, 25 (2021).
 - [40] S. V. Scarpino and G. Petri, *Nat. Commun.* **10**, 055101(R) (2020), arXiv:1703.07317.
 - [41] W. Cai, L. Chen, F. Ghanbarnejad, and P. Grassberger, *Nat. Phys.* **11**, 936 (2015).
 - [42] L. Chen, F. Ghanbarnejad, W. Cai, and P. Grassberger, *Epl* **104**, 10.1209/0295-5075/104/50001 (2013), arXiv:1307.2404.
 - [43] J. Kim, P. L. Krapivsky, B. Kahng, and S. Redner, *Phys. Rev. E - Stat. Physics, Plasmas, Fluids, Relat. Interdiscip. Top.* **66**, 055101(R) (2002), arXiv:0203167 [cond-mat].
 - [44] Y. S. Cho, J. S. Kim, J. Park, B. Kahng, and D. Kim, *Phys. Rev. Lett.* **103**, 135702 (2009).
 - [45] G. Bianconi and P. L. Krapivsky, *Phys. Rev. E* **102**, 032305 (2020), arXiv:2004.03934.
 - [46] D. Scarselli, N. B. Budanur, M. Timme, and B. Hof, *Nat. Commun.* **12**, 10.1038/s41467-021-22725-9 (2021).
 - [47] R. Pastor-Satorras and A. Vespignani, *Phys. Rev. E - Stat. Physics, Plasmas, Fluids, Relat. Interdiscip. Top.* **65**, 036104 (2002), arXiv:0107066 [cond-mat].
 - [48] L. Hébert-Dufresne, A. Allard, J.-G. Young, and L. J. Dubé, *Sci. Rep.* **3**, 2171 (2013), arXiv:1208.5768.
 - [49] R. Cohen, S. Havlin, and D. ben-Avraham, *Phys. Rev. Lett.* **91**, 247901 (2003), arXiv:0207387 [cond-mat].
 - [50] Z. Ghalmane, M. E. Hassouni, and H. Cherifi, *Soc. Netw. Anal. Min.* **9**, 1 (2019).
 - [51] S. Osat, A. Fagheh, and F. Radicchi, *Nat. Commun.* **8**, 1 (2017), arXiv:1707.01401.
 - [52] C. M. Schneider, T. Mihaljev, S. Havlin, and H. J. Herrmann, *Phys. Rev. E* **84**, 061911 (2011), arXiv:1102.1929.
 - [53] G. S. Costa and S. C. Ferreira, *Phys. Rev. E* **101**, 022311 (2020), arXiv:1912.09976.
 - [54] S. Yan, S. Tang, W. Fang, S. Pei, and Z. Zheng, *J. Stat. Mech. Theory Exp.* **2015**, 10.1088/1742-5468/2015/08/P08010 (2015).
 - [55] P. Clusella, P. Grassberger, F. J. Pérez-Reche, and A. Politi, *Phys. Rev. Lett.* **117**, 208301 (2016), arXiv:1604.00073.
 - [56] N. Masuda, *New J. Phys.* **11**, 0 (2009), arXiv:0909.1945.
 - [57] P. Van Mieghem, D. Stevanović, F. Kuipers, C. Li, R. van de Bovenkamp, D. Liu, and H. Wang, *Phys. Rev. E - Stat. Nonlinear, Soft Matter Phys.* **84**, 016101 (2011).
 - [58] J. T. Matamalas, A. Arenas, and S. Gómez, *Sci. Adv.* **4**, eaau4212 (2018), arXiv:1711.10443.
 - [59] Z. Dong, Y. Chen, T. S. Tricco, C. Li, and T. Hu, in *2020 IEEE Intl Conf Parallel Distrib. Process. with Appl. Big Data Cloud Comput. Sustain. Comput. Commun. Soc. Comput. Netw.* (IEEE, 2020) pp. 845–851.
 - [60] Y. Chen, G. Paul, S. Havlin, F. Liljeros, and H. E. Stanley, *Phys. Rev. Lett.* **101**, 058701 (2008).
 - [61] N. Madar, T. Kalisky, R. Cohen, D. ben-Avraham, and S. Havlin, *Eur. Phys. J. B* **38**, 269 (2004).
 - [62] K. Dietz, *Stat. Methods Med. Res.* **2**, 23 (1993).
 - [63] Y. Alimohamadi, M. Taghdir, and M. Sepandi, *J. Prev. Med. Public Heal.* **53**, 151 (2020).
 - [64] J. Ma, *Infect. Dis. Model.* **5**, 129 (2020).
 - [65] J. L. Doob, *Trans. Am. Math. Soc.* **52**, 37 (1942).
 - [66] D. T. Gillespie, *J. Comput. Phys.* **22**, 403 (1976).
 - [67] K. I. Goh, B. Kahng, and D. Kim, *Phys. Rev. Lett.* **87**, 278701 (2001), arXiv:0106565 [cond-mat].
 - [68] J. S. Lee, K. I. Goh, B. Kahng, and D. Kim, *Eur. Phys. J. B* **49**, 231 (2006).
 - [69] D. H. Kim, J. Park, and B. Kahng, *PLoS One* **12**, e0184683 (2017), arXiv:1608.01071.
 - [70] D. Lee, B. Kahng, Y. S. Cho, K. I. Goh, and D. S. Lee, *J. Korean Phys. Soc.* **73**, 152 (2018), arXiv:1808.00905.
 - [71] K. I. Goh, G. Salvi, B. Kahng, and D. Kim, *Phys. Rev. Lett.* **96**, 018701 (2006), arXiv:0508332 [cond-mat].
 - [72] S. H. Yook and Y. Kim, *Phys. Rev. E* **97**, 042317 (2018).
 - [73] D. Mistry, M. Litvinova, A. Pastore y Piontti, M. Chinazzi, L. Fumanelli, M. F. Gomes, S. A. Haque, Q. H. Liu, K. Mu, X. Xiong, M. E. Halloran, I. M. Longini, S. Merler, M. Ajelli, and A. Vespignani, *Nat. Commun.* **12**, 1 (2021), arXiv:2003.01214.
 - [74] T. Kim and B. K. Kim, *Inter-Asia Cult. Stud.* **21**, 533 (2020).
 - [75] M. Ryan, *Int. J. Pervasive Comput. Commun.* **16**, 383 (2020).
 - [76] Y. Park, Y. Choe, O. Park, S. Y. Park, Y. M. Kim, J. Kim, S. Kweon, Y. Woo, J. Gwack, S. S. Kim, J. L. Hyun, B. Ryu, Y. Sukjang, H. Kim, S. H. Shin, S. Yi, S. Lee, H. K. Kim, H. Lee, Y. Jin, E. Park, S. W. Choi, M. Kim, J. Song, S. W. Choi, D. Kim, B. H. Jeon, H. Yoo, and E. Kyeongjeongm, *Emerg. Infect. Dis.* **26**, 2465 (2020).
 - [77] H. Ko, J. Leitner, E. Kim, and J. Jeong, *Int. Data Priv. Law* **7**, 100 (2017).
 - [78] K. Choi, H. Choi, and B. Kahng, arXiv preprint arXiv:2010.07157, 1 (2020), arXiv:2010.07157.
 - [79] W. Lee, S.-S. Hwang, I. Song, C. Park, H. Kim, I.-K. Song, H. M. Choi, K. Prifti, Y. Kwon, J. Kim, S. Oh, J. Yang, M. Cha, Y. Kim, M. L. Bell, and H. Kim, *Int. J. Epidemiol.* **49**, 1106 (2020).
 - [80] K.-D. Min, H. Kang, J.-Y. Lee, S. Jeon, and S.-i. Cho, *J. Korean Med. Sci.* **35**, 1 (2020).
 - [81] C. Runge, *Math. Ann.* **46**, 167 (1895).
 - [82] W. Kutta, *Zeit. Math. Phys.* **46**, 435 (1901).
 - [83] S. Kirkpatrick, C. Gelatt, and M. Vecchi, in *Readings Comput. Vis.*, 4598 (Elsevier, Berlin, Heidelberg, 1987) pp. 606–615.
 - [84] J. Mossong, N. Hens, M. Jit, P. Beutels, K. Auranen, R. Mikolajczyk, M. Massari, S. Salmaso, G. S. Tomba, J. Wallinga, J. Heijne, M. Sadkowska-Todys, M. Rosinska, and W. J. Edmunds, *PLoS Med.* **5**, e74 (2008).